The “Ocular Response Function” for encoding and decoding oculomotor related neural activity

Quirin Gehmacher [1,2*], Juliane Schubert [3], Aaron Kaltenmaier [1,2], Nathan Weisz [3,4], Clare Press [1,2]

[1] Department of Experimental Psychology, University College London, WC1H 0AP, United Kingdom.
[2] Department of Imaging Neuroscience, UCL Queen Square Institute of Neurology, University College London, WC1N 3AR, United Kingdom.
[3] Paris-Lodron-University of Salzburg, Department of Psychology, Centre for Cognitive Neuroscience, Salzburg, Austria.
[4] Neuroscience Institute, Christian Doppler University Hospital, Paracelsus Medical University, Salzburg, Austria.

*Corresponding Author: q.gehmacher@ucl.ac.uk

Abstract

Oculomotor activity provides critical insights into cognition and health, with growing evidence demonstrating its involvement in various cognitive functions such as attention, memory, and sensory processing. Furthermore, eye movements are emerging as significant indicators of psychopathologies and neurological disorders, including schizophrenia, dementia, depression, and tinnitus. Despite its crucial importance across domains, the role of oculomotion has often been underexplored in neuroimaging studies - largely due to methodological challenges. Eye movements have traditionally been viewed as artefacts in the neural signal, leading to the exclusion of epochs containing them, or correction methods to remove their influence. However, this strategy does not allow us to determine their role in a range of neural effects or mapping between tasks and neural responses. To enable such nuanced investigations in typical function and disease, we introduce what we term “Ocular Response Functions”. We used simultaneous magnetoencephalographic and eye-tracking recordings during the resting-state combined with temporal response functions to precisely map the relationship between oculomotion and neural activity. Our approach allows for the temporally and spatially precise prediction of neural activity based on ocular action, and vice versa. We further validate this method in a passive listening task, highlighting its potential for uncovering cognitive insights in experimental settings. By providing a robust framework for examining the interplay between eye movements and neural processes, our method opens new avenues for both research and clinical applications, potentially advancing early detection and intervention strategies for neurological and psychiatric disorders.

Introduction

Oculomotor activity offers a unique opportunity for understanding key aspects of cognition and health [1], with recent demonstrations that it plays a key role in a wide range of cognitive functions, including attention, memory, visual, and auditory processing [2–15]. Relatedly, it is increasingly being recognized as an important indicator of psychopathology and neurological disorders, with links to conditions such as schizophrenia [16–21], dementia [22–26], and depression [27–30], and even phantom perceptions like tinnitus [31–33].

However, despite the likely crucial contribution of oculomotor activity across domains, studying its role has proven difficult methodologically. Traditionally, eye movements were often viewed as confounding variables in neuroimaging due to muscular artefacts that can contaminate the neural signal. Such confounds have led typically to their exclusion from data analysis - initially via excluding periods of the neural signal including eye movements, and more recently, via methods like Independent Component Analysis (ICA). As a result, their potential role in shaping neural dynamics has been frequently overlooked.

In spite of these difficulties with measurement, it is evident that eye movements will directly influence underlying neural activation patterns [2,3,6,8,34], with a range of motoric and midbrain structures necessary for generation and sensory processing as both cause and effect. Understanding oculomotor behaviour's precise role in shaping these neural processes offers a way to gain deeper insights into brain function, refining our interpretation of neural data and advancing knowledge of both cognitive function and disease mechanisms. This understanding could also be crucial in enhancing the early detection of psychopathological and neurological disorders.

To enable such crucial investigations in typical functioning and disease, there is a pressing need for advanced tools and methodologies that can reliably isolate and account for the effects of eye movements on neural activity. Such approaches are essential for disentangling the intricate dynamics between eye movements and neural activation, leading to more accurate neuroimaging interpretations. Ultimately, this understanding could help to identify neural signatures linked to both typical cognitive processes and psychopathologies, paving the way for more targeted diagnostic and therapeutic interventions.

To this end, we thus developed a method that would precisely elucidate the role of ocular activity in neural processes across time. We employed simultaneous human magnetoencephalographic (MEG) and eye-tracking recordings during the resting-state,

combined with temporal response functions (TRFs), to derive transfer functions that link oculomotion to neural activity. These ocular response functions (ORFs) allow us to both predict neural activity from ocular action and, conversely, predict ocular action from brain activity. By applying saccade ORFs to a passive listening task, we establish a "proof-of-principle" that ORFs extend beyond the specific dataset or condition on which they were trained, demonstrating their versatility in uncovering relationships between ocular action and neural activity even in contexts where eye movements are not typically expected to influence cognitive processing. This indicates that ORFs can capture subtle links between ocular dynamics and brain activity, showcasing the cognitive insights this method offers during experimental manipulations. We thus hope to provide a powerful new tool for understanding the complex role of oculomotor-related signals in human cognition, offering new avenues for both research and clinical applications.

Results

In the following, we present the 'Ocular Response Function' method and organise the results into three sections. First, we outline the general steps for estimating ORFs, providing a schematic overview of the rationale and methodology behind their calculation, and how they can be used to predict brain activity from ocular action (encoding) or ocular action from brain data (decoding). Second, we show that source-projected ORFs account for variance across distinct brain regions, each characterised by unique temporal profiles, both in data with and without oculomuscular artefact correction (ICA and no-ICA). By convolving resting-state data with the corresponding ORFs, we demonstrate that brain activity can be reliably predicted from ocular action and vice versa. Third, we extend the ORF method to data from a passive listening task, demonstrating that the approach can be applied to experimental conditions beyond the resting state, offering insights into how oculomotor processes contribute to neural activity during cognitive tasks. This section highlights the generalizability of ORFs across different paradigms, enabling their application in various experimental contexts.

The 'Ocular Response Function'

Establishing an eye - response relationship for time-continuous input, the ORF leverages the functionality behind a deconvolution algorithm [35] (boosting, see Fig. 1A) as implemented in the Eelbrain toolkit [36]. To estimate the ORFs that best describe the unique relationship between each individual eye feature (i.e. horizontal and vertical gaze, pupil dilation, blinks, and saccades) and neural responses in a time-resolved manner, we predicted brain activity from all eye features in the same forward encoding model (see Fig. 1B). The data were collected from a 5-minute period where participants had no task other than to direct their

gaze toward a black cross at the centre of a screen. Fitting these models to resting-state data of individual participants allows for an estimation of response functions in the absence of any experimental confound by stimulation, task, or both (see Fig. 1C). This is repeated for each of 306 MEG sensors, leading to one response function per eye feature per sensor. In a nutshell, the ORF reflects the strength of the physiological relationship between the eye and MEG signals at different temporal offsets of the eye and MEG time-series. For example, the value at +100 ms indicates the correlation between time-series when the neural time-series follows the eye time-series by 100 ms, thereby reflecting the brain's response to eye events. Conversely, the value at -100 ms represents the correlation when the neural time-series precedes the eye one, thereby reflecting neural activity leading to the occurrence of these eye events.

Once the ORFs are estimated, the process can be reversed to create decoding models, simply flipping the temporal axis of ORFs to predict eye movements from the recorded brain signals. This backward decoding is instrumental in understanding how neural patterns can be used to infer ocular behaviour, thereby contributing to a bidirectional understanding of brain-eye interactions. Models were fitted to neural data that were either cleaned from oculomuscular (and cardiac) artefacts via ICA or where those components were retained (no-ICA) - providing the opportunity to further differentiate between contributions of oculomuscular and oculomotor neural activity to M/EEG recordings. To localise these effects, the ORFs were projected into source space. This source projection helps map the ORFs from the sensor level to likely generators, allowing for anatomical localization of the response functions. Here, we then minimise the number of statistical comparisons, while identifying the most relevant components of the neural response across space and time, by applying principal component analysis (PCA) to the source projected ORFs. For evaluation and application to other experimental tasks, we first convolve each eye movement feature with the corresponding source-projected ORFs. This generates a time course of predicted brain activity for each voxel, based on the eye movement data. We then correlate these predicted time courses with the actual source-projected brain recordings, yielding a correlation coefficient for each voxel. This coefficient reflects the extent to which information about the eye movement is preserved at that specific brain location (encoding, see Fig. 2A). Conversely, by flipping the ORFs of each individual eye movement, we convolve them with source-projected brain recordings to generate a time course of predicted eye movement activity. The extent to which ocular behaviour can be inferred from brain activity is then calculated by correlating the predicted eye movement data with the actual recordings (decoding; see Fig. 2B).

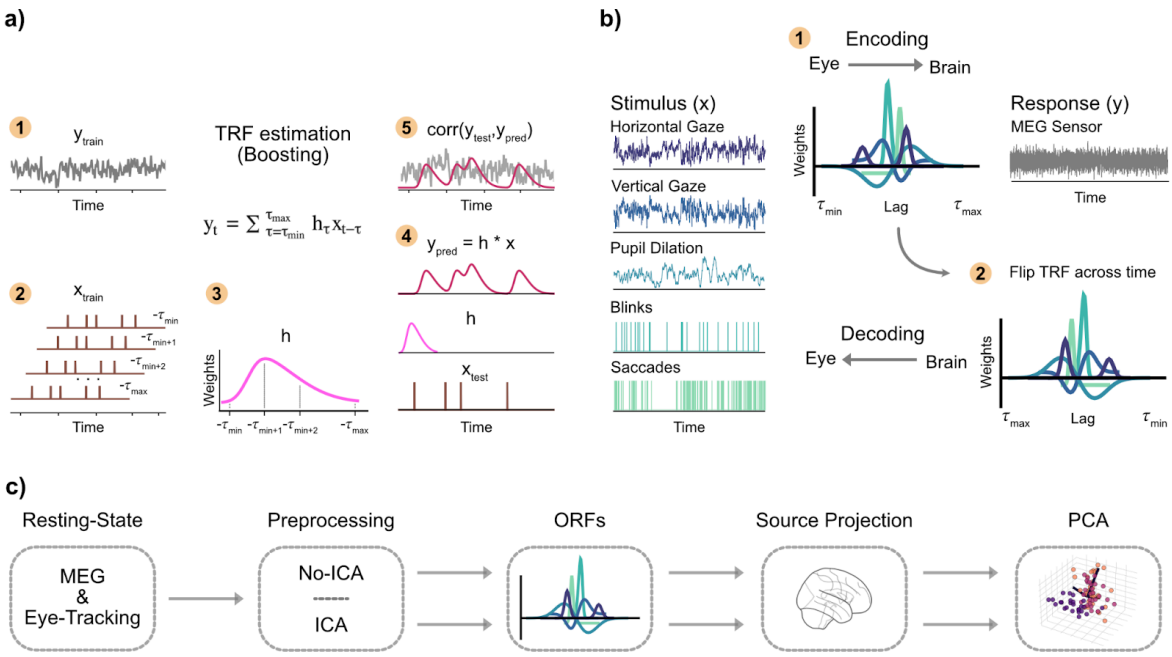

Fig. 1: *The Ocular Response Function*. **a)** Eye (x) - response (y) relationships are estimated using deconvolution (Boosting), where neural activity (y_{train}) is linked to an ocular action (x_{train}, e.g. saccades) with time-shifted versions to capture the brain's delayed response. The TRF (filter kernel, h) represents how the brain processes the stimulus over time. This filter is then applied (using convolution) to new stimulus data (x_{test}) to predict the neural response (y_{pred}). Finally, the predicted response is compared to the actual neural activity (y_{test}) to assess the model fit and evaluate how accurately the TRF captures the brain's response dynamics. **b)** Ocular response functions (ORFs) leverage this approach by predicting resting state brain activity from various eye features (horizontal gaze, vertical gaze, pupil dilation, blinks, saccades) using a forward encoding model. One ORF is generated per eye feature per sensor. To predict eye movements from brain data, the ORF is simply flipped along the temporal axis. **c)** Models were fitted to neural resting-state data either cleaned of oculomuscular and cardiac artefacts (ICA) or with these components retained (no-ICA), enabling differentiation between neural and muscular activity. While other approaches are possible, in the present study, ORFs were projected into source space for anatomical localization, with principal component analysis (PCA) applied to identify key neural components across space and time, minimising statistical comparisons. This represents one application of the method to explore neural responses.

To summarise the results, we conducted a principal component analysis (PCA) and examined the topographies and sources of the first three principal components based on the maximum explained variance, uncovering the contributions of distinct brain regions to encoding and decoding ocular action (see Fig. 2C&D). In the following, we present distinct ORF time courses for the first component, along with encoding effects at the locations of maximum weight. Additionally, decoding effects are demonstrated by predicting eye movement patterns using all source-projected ORFs, either collectively or weighted by the PCA matrices of the first component (for components two and three please refer to the Supplementary Material, Supplementary Figures, Fig. 3-5).

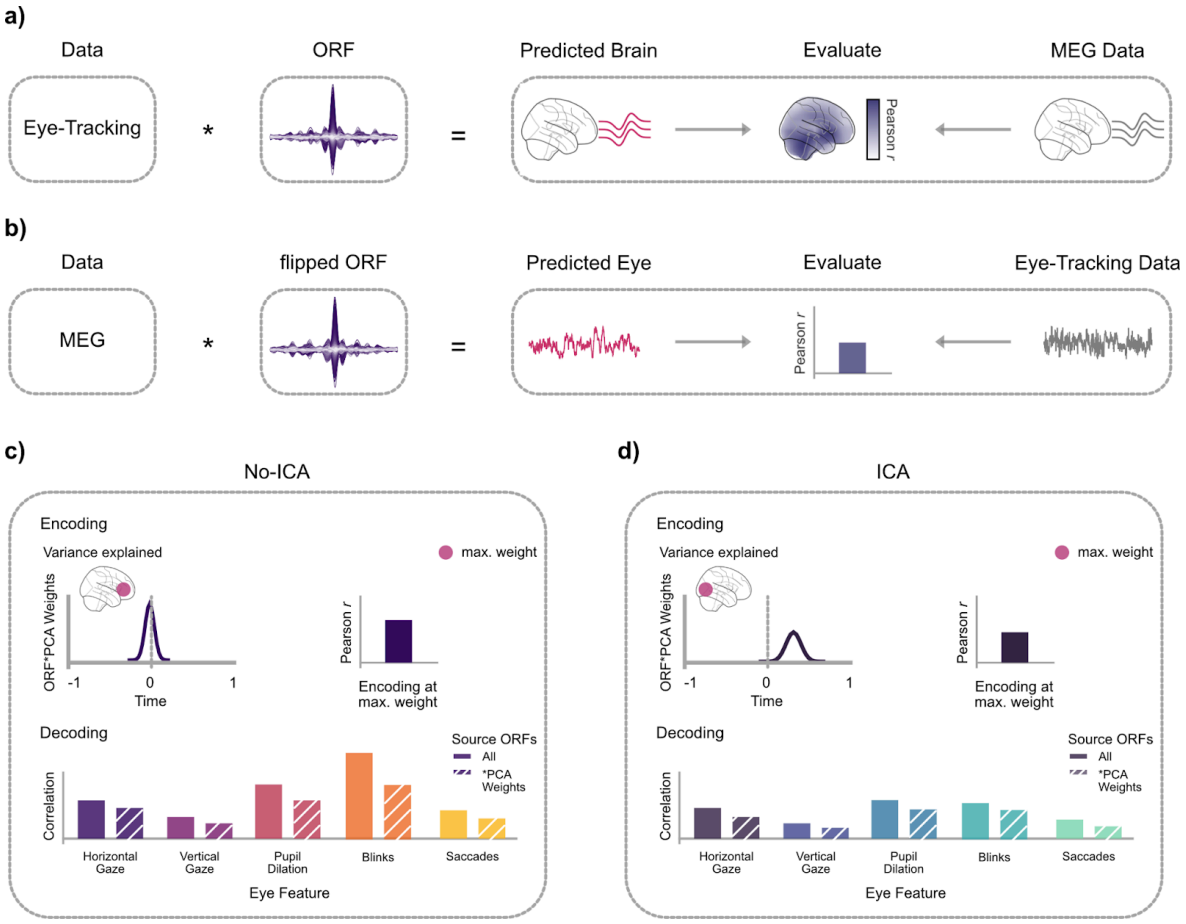

Fig. 2: *The approach for obtaining encoding and decoding results*. **a)** Encoding results are obtained by convolving eye-tracking data with corresponding ORFs to generate predicted brain activity across the same channel dimensions. The predicted activity is then compared with actual neural recordings to evaluate model fit for every channel (e.g., using Pearson correlation), indicating how much information of an eye feature is captured in the brain data. **b)** Similarly, eye features can be predicted from brain activity by convolving the actual neural data with time-reversed ORFs, generating predicted eye patterns. Model fit is assessed by comparing the predicted and actual eye-tracking data, resulting in a single coefficient (e.g., Pearson correlation). **c & d)** To summarise the results, we analysed the contributions of different brain regions by weighting the ORFs from both no-ICA and ICA data using PCA weight matrices. This method highlights the roles of distinct brain regions in encoding and decoding ocular behaviour, while reducing statistical complexity. For the no-ICA data, we anticipated that most variance would be captured by frontal regions with earlier temporal peaks, reflecting muscular contributions. To ensure that the observed effects were consistent across participants and not driven by individual variability, we examined the encoding effects for each participant at the voxel with the highest component weight. In the ICA-cleaned data, we expected more distributed effects in cerebellar and motor structures, as well as sensory regions with delayed temporal peaks, as muscular artefacts were removed.

Ocular response functions, encoding, and decoding during the resting state

First, we established ORFs through the prediction of resting-state brain activity, with and without oculomuscular artefact correction (ICA and no-ICA), based on five eye features: horizontal and vertical gaze, pupil dilation, blinks, and saccades. We weighted the ORFs using the PCA weight matrices of the first principal components.

In brain data without ICA preprocessing, the first principal component generally exhibited stronger loadings over frontocentral regions, particularly near the eyeballs. In contrast, after applying ICA, the loadings shifted toward cerebellar and subcortical structures. Additionally, the temporal patterns in the no-ICA data tended to peak earlier than those in the ICA-processed data. Of course, the ICA cannot perfectly dissociate muscular artefacts from neural signals given it is only correlation-based, but by removing the components with frontal topographies, the ICA analysis allows the patterns in other (not frontocentral) neural structures to be observed more readily. Below, we present the temporal patterns and encoding results for the no-ICA data, followed by a similar analysis for the ICA-processed data.

No-ICA Preprocessing. For horizontal gaze, the first component (explained variance: μ = 59.7%, *sd* = 21.4%) peaked just before 0 ms, suggesting an almost instantaneous relationship between the particular neural pattern and eye movements. Encoding across participants was significant at the voxel of maximum weight - evaluated by a one-sample Student's t-test (r = 0.10, $t(28)$ = 6.33, p < 0.001, Cohen's d = 1.17; see Fig. 3a), indicating that frontocentral regions reflect shifts in horizontal gaze. Vertical gaze showed a more spatially widespread pattern (explained variance: μ = 56.6%, *sd* = 11.8%), but with maximum loadings over regions similar to those observed for horizontal gaze, and a comparable temporal pattern (r = 0.03, t(28) = 2.51, p = 0.018, Cohen's d = 0.47; see Fig. 3b; note that while the peak fell at the olfactory lobe here the glass brains indicate that the pattern is rather similar to horizontal gaze). For pupil dilation (explained variance: μ = 60.5%, *sd* = 17.1%) it exhibited a clear peak from ~ -500 to -300 ms, suggesting frontocentral changes associated with pupil diameter modulation by approximately 300-500 ms later (r = 0.05, $t(28)$ = 7.95, p < 0.001, Cohen's d = 1.48; see Fig. 3c). For eye blinks (explained variance: μ = 94.2%, *sd* = 3.5%) it peaked just before 0 ms, like with horizontal eye movements (r = 0.50, $t(28)$ = 16.37, p < 0.001, Cohen's d = 3.04; see Fig. 3d). Finally, the first component for

saccadic eye movements (explained variance: μ = 26.7%, *sd* = 19.1%) exhibited widespread loadings over frontal, midbrain, and subcortical regions, peaking at ~100 ms. This suggests that frontocentral regions also reflect the initiating and registering of saccades (r = 0.11, $t(28)$ = 7.73, p < 0.001, Cohen's d = 1.44; see Fig. 3e). Therefore, without ICA preprocessing, the first principal component for all eye features originates from frontocentral sources - likely driven by the muscles controlling the eyeballs - exhibiting varying time courses depending on specific behaviours.

ICA Preprocessing. After ICA preprocessing, the first component for each eye feature maximally loaded over the cerebellum. For horizontal gaze, the first component (explained variance: μ = 43.9%, *sd* = 13.7%) peaked around 80 - 100 ms, indicating a delayed neural response relative to the horizontal gaze shift (r = 0.05, $t(28)$ = 10.83, p < 0.001, Cohen's d = 2.01; see Fig. 3f). Vertical gaze (explained variance: μ = 65.8%, *sd* = 16.8%) showed a similar temporal pattern but did not reach significance (r = -0.00, $t(28)$ = -0.19, p = 0.850, Cohen's d = 0.04; see Fig. 3g), suggesting that the brain's response to vertical gaze is either more diffuse or less tied to specific regions. Pupil dilation (explained variance: μ = 52.3%, *sd* = 13.5%) showed sustained activity from ~-500 to 250 ms, reflecting prolonged connectivity between cerebellar and subcortical regions and pupil diameter changes (r = 0.03, $t(28)$ = 8.38, p < 0.001, Cohen's d = 1.56; see Fig. 3h). Eye blinks (explained variance: μ = 64.8%, *sd* = 16.3%) exhibited two peaks, at ~30 ms and ~200 ms, indicating a delayed neural response relative to the blink (r = 0.10, $t(28)$ = 9.61, p < 0.001, Cohen's d = 1.78; see Fig. 3i). For saccades, the first component (explained variance: μ = 59.1%, *sd* = 19.4%) peaked at ~100 ms, again reflecting a delayed neural response (r = 0.08, $t(28)$ = 10.51, p < 0.001, Cohen's d = 1.95; see Fig. 3j).

The second and third component for all eye features showed loadings over parietal and sensory regions, with significant encoding at the voxels of maximum weight across participants. This suggests that other brain areas, such as occipital regions, also play important roles in ocular behaviour. For detailed results concerning these components, including visualisations, please refer to the Supplementary Material (Supplementary Figures, Fig. 1&2).

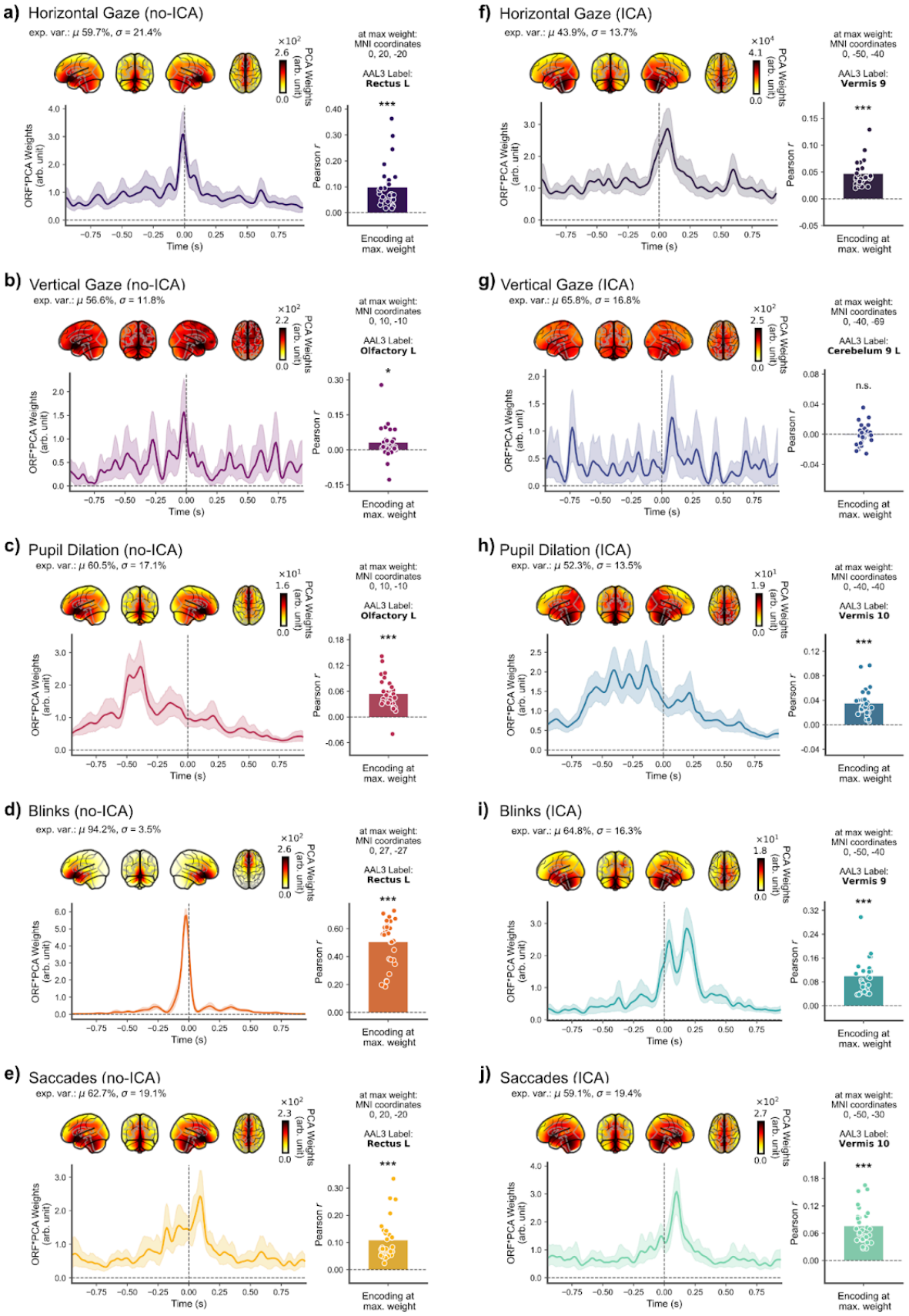

Fig. 3: *Encoding and PCA results of the first component for eye features with and without oculomuscular artefact correction (ICA vs. no-ICA)*. No-ICA results: All No-ICA first components

were localised to frontocentral or olfactory structures, likely associated with muscular artefacts as much as real neural signals. **a)** For horizontal gaze, it peaked just before 0 ms **b)** Vertical gaze showed a broader spatial distribution but similar temporal patterns. **c)** Pupil dilation showed a prominent peak ~300 - 500 ms before the pupil response. **d)** Eye blinks exhibited nearly instantaneous effects. **e)** Saccades were associated with widespread frontocentral, midbrain, and subcortical localisations, peaking at ~100 ms. Given that it is likely that these ORFs are largely associated with muscular artefacts, we performed the same analyses with ICA correction for this. After such ICA correction, the encoding patterns shifted to more posterior and subcortical regions, with peaks localised to the cerebellum. **f)** Horizontal gaze showed a delayed response peaking at ~80 - 100 ms. **g)** Vertical gaze followed a similar delayed pattern but did not reach significance. **h)** Pupil dilation reflected a sustained response from 500 to 250 ms. **i)** Eye blinks displayed dual peaks (~30 ms and ~200 ms), indicating delayed neural activity. **j)** Saccades also showed delayed activity peaking at ~100 ms. Shaded error bars represent 95% CI's. Anatomical labels were obtained using the automated anatomical labelling atlas 3 (AAL3). Statistics were performed using one-sample Student's t-tests. 'n.s.': not significant; '*': $p < 0.05$; '**': $p < 0.01$; '***': $p < 0.001$. $N = 29$.

Next, we assessed the extent to which eye features could be decoded from neural data, either using whole-brain information or PCA-based methods. The decoding was evaluated by comparing the actual eye feature time series to predictions generated from neural data. These predictions were obtained by convolving source-projected brain data with source-projected ocular response functions (ORFs) using five convolution methods: the full dataset ('All'), by multiplying the PCA weight matrix with both the source-projected brain data and ORFs (*PCA Weights'), or by using the PCA weights from the first ('*PCA W1'), second ('*PCA W2'), or third ('*PCA W3') components. We calculated correlation coefficients (Pearson's r for horizontal gaze, vertical gaze, and pupil dilation, and Matthew's Correlation Coefficient (MCC) for blinks and saccades) between the actual and predicted eye movements.

In this section, we focus on the decoding results using the more 'traditional' approach based on all source ORFs ('All') and decoding ocular behaviour using data reduced to the spatially localised activation patterns of the first principal component ('*PCA W1'). For complementary decoding results using the other convolution methods ('*PCA Weights', '*PCA W2', '*PCA W3'), as well as visualisations and summary statistics, please refer to the Supplementary Material (Supplementary Figures, Fig. 3-5 & Supplementary Tables, Table 1-5).

Overall, ocular behaviour was reliably decoded across all eye features and preprocessing strategies (no-ICA, see Fig. 4a; ICA, see Fig. 4b).

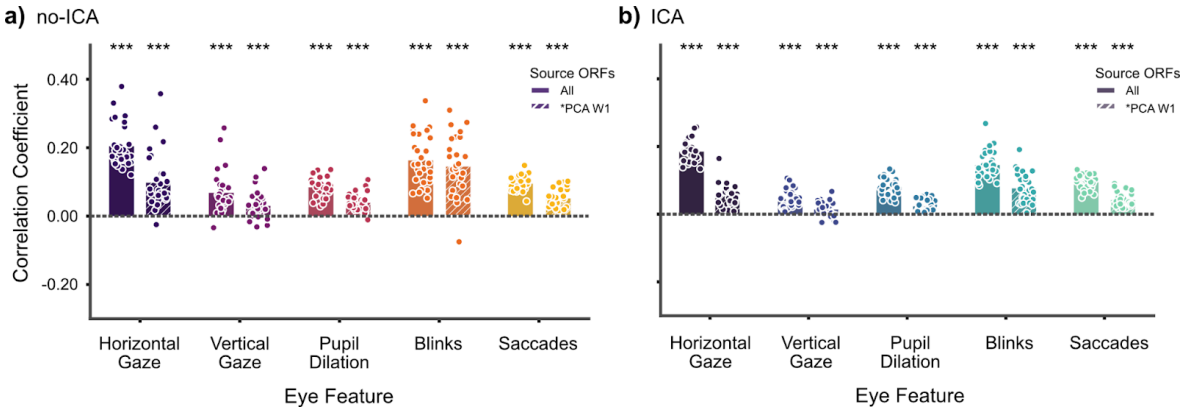

Fig. 4: *Eye features can be reliably decoded from resting state neural activity using source-projected ORFs and PCA-reduced data*. **a)** No-ICA preprocessing: Ocular behaviour was reliably decoded using both all source-projected ORFs ('All') and PCA-reduced data ('*PCA W1'). For 'All' source ORFs, horizontal gaze showed strong decoding accuracy (r = 0.20, p < 0.001), followed by vertical gaze (r = 0.07, p < 0.001), pupil dilation (r = 0.08, p < 0.001), blinks (MCC = 0.16, p < 0.001), and saccades (MCC = 0.09, p < 0.001). The '*PCA W1' results demonstrated a reduction in decoding performance across all features, but the relationships remained significant: horizontal gaze (r = 0.10, p < 0.001), vertical gaze (r = 0.03, p = 0.001), pupil dilation (r = 0.04, p < 0.001), blinks (MCC = 0.14, p < 0.001), and saccades (MCC = 0.05, p < 0.001). **b)** ICA preprocessing: Decoding accuracy remained high across all eye features. For 'All' source ORFs, horizontal gaze exhibited strong decoding performance (r = 0.18, p < 0.001), followed by vertical gaze (r = 0.04, p < 0.001), pupil dilation (r = 0.08, p < 0.001), blinks (MCC = 0.15, p < 0.001), and saccades (MCC = 0.10, p < 0.001). With '*PCA W1' data, decoding performance was reduced but still significant for all features: horizontal gaze (r = 0.05, p < 0.001), vertical gaze (r = 0.02, p = 0.001), pupil dilation (r = 0.03, p < 0.001), blinks (MCC = 0.08, p < 0.001), and saccades (MCC = 0.04, p < 0.001). Statistics were performed using one-sample Student's t-tests. 'n.s.': not significant; '*': p < 0.05; '**': p < 0.01; '***': p < 0.001. N = 29.

These analyses indicate that neural signals associated with ocular behaviour contain sufficient information to predict eye movements, even after removing oculomuscular related variance in brain recordings. It further implies that eye movements can also be reliably decoded when the data is reduced to more localised spatial-temporal response patterns.

Ocular response functions uncover the differences and overlap of task-related oculomotor and neural activity

We then applied the proposed ORF logic to a passive listening task that was performed after the resting state recordings, where randomly or regularly ordered sequences of tones were presented. This analysis serves as a "proof-of-principle," demonstrating that ORFs generalise beyond the specific dataset or condition on which they were trained. Additionally, it highlights their versatility in uncovering relationships between ocular actions and neural activity, even in contexts like passive listening, where eye movements are not typically expected to influence cognitive processing. Participants were again instructed to direct their gaze toward a black cross at the centre of a screen while passively listening to the tone

sequences with varying regularity. Each block consisted of 1500 tones (440 Hz, 587 Hz, 782 Hz, or 1043 Hz) presented at a rate of 3 Hz. The Regularity conditions (ordered and random) alternated every 500 trials. In the 'ordered' condition, forward transitions of moving up one pitch step were more likely (75%) and repetitions were less likely (25%), whereas in the 'random' condition all transitions occurred with equal probability (25%). To decode the regularity conditions from neural activity, we performed multivariate pattern analysis (MVPA) with 5-fold cross-validation, assessing classification performance across time windows from -100 ms to 400 ms relative to tone onset (see Fig. 5A). This analysis revealed that task-related neural activity exhibited distinct patterns that reliably differentiated between ordered and random auditory sequences, demonstrating the brain's sensitivity to changes in stimulus regularity.

Cluster-based permutation tests comparing actual classification performance with a control analysis using shuffled class labels showed significant differences in regularity processing between 100 and 190 ms post-tone onset ($t(27) = 3.61$, $p < 0.001$, Cohen's $d = 0.68$; see Fig. 5B). Importantly, neural activity related to saccadic eye movements also differentiated between the ordered and random conditions, with a significant cluster spanning the entire classifier time window ($t(27) = 2.52$, $p = 0.010$, Cohen's $d = 0.48$). This suggests that while saccadic behaviour is less tightly time-locked to specific stimulus onsets, it nonetheless shows a distinct and consistent engagement between the ordered and random conditions that may contribute to the neural classification results (interestingly, saccade rates suggest greater engagement in saccadic behaviour during the ordered condition, see Supplementary Figures Fig. 6).

This classification was based on predicted neural activity generated by convolving saccadic eye movements during the task with ORFs derived from the resting-state recordings. This approach allowed us to isolate and assess MEG activity related specifically to saccades during passive listening, providing a precise measure of how oculomotor dynamics influence task-related neural signals. We specifically targeted saccades for this analysis due to recent findings linking neural excitability in the auditory cortex with saccades [37].

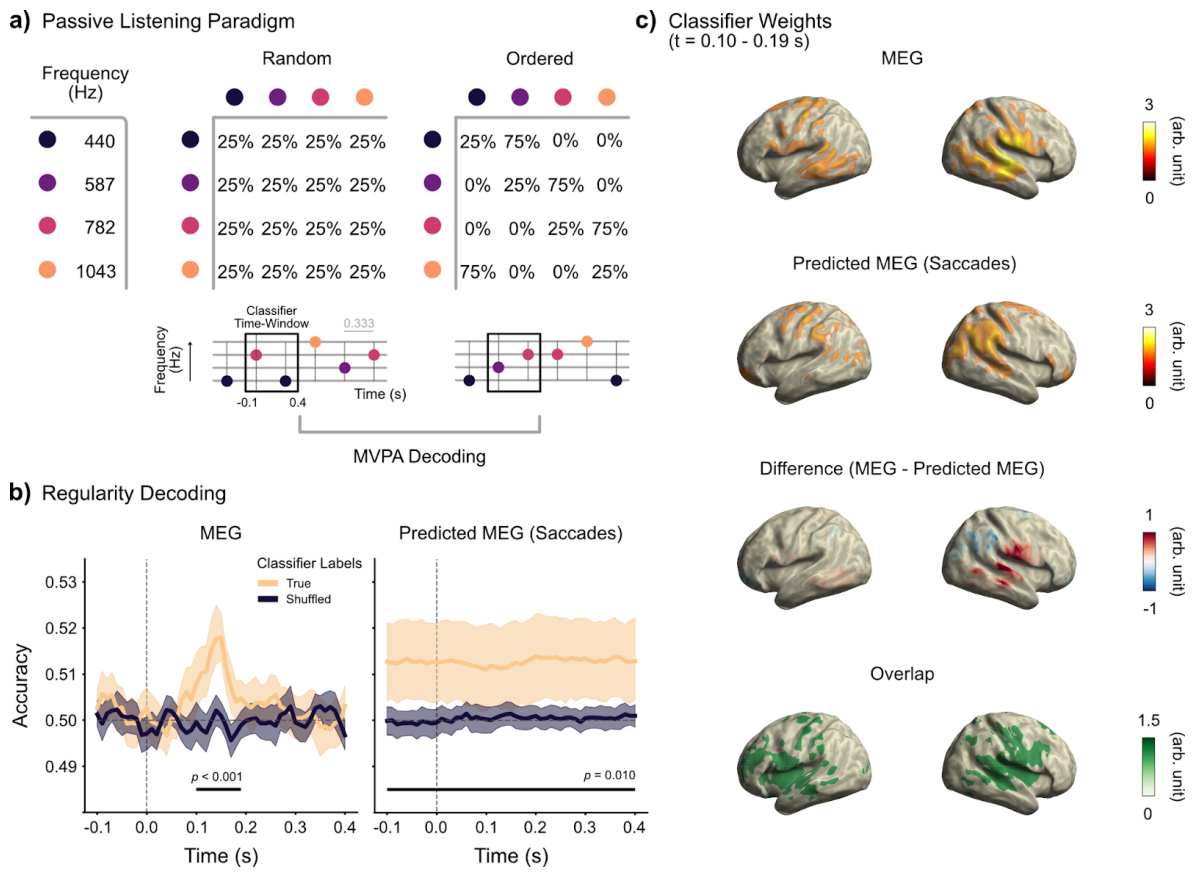

Fig. 5: *Uncovering the differences and overlap of task-related oculomotor and neural activity using ocular response functions*. **a)** Participants passively listened to tone sequences while maintaining their gaze on a central fixation cross. Tones were presented at a rate of 3 Hz in either an ordered or random sequence, with regularity condition alternating every 500 trials. Multivariate pattern analysis (MVPA) with 5-fold cross-validation was used to decode neural responses to ordered and random sequences from MEG data. **b)** Decoding was applied to both actual MEG data and predicted MEG data, generated by convolving saccadic eye movements with ORFs derived from resting-state recordings. This method allowed us to isolate the neural contributions of saccadic behaviour to the classification process. Cluster-based permutation tests revealed significant decoding differences between ordered and random tones in MEG data (100 - 190 ms, $p < 0.001$). Saccadic eye movements also differentiated conditions (-100 - 400ms, $p = 0.010$), though less time-locked to stimulus onset across participants. **c)** Classifier weights, averaged across the significant MEG decoding cluster (100 - 190 ms) and projected into source space. For MEG, classifier weights revealed informative activity to mainly originate from auditory cortices, with a right hemispheric dominance. The overlap in midbrain, temporal and parietal regions suggests shared neural mechanisms for encoding regularity from both auditory and saccade-related activity, and hence the potential mechanistic role of saccades in mediating some of the auditory response. Weights were thresholded at 75% for visualisation purposes. 'n.s.': not significant; '*': $p < 0.05$; '**': $p < 0.01$; '***': $p < 0.001$. $N = 28$.

Given that saccade-related neural activity during the passive listening task also differentiated between regularity conditions, we sought to explore how these oculomotor processes and general task-related neural processes might be related. Specifically, we were interested in understanding how these processes both differ and overlap, as they are not mutually exclusive. To investigate this, we compared the neural patterns associated with task-related MEG signals and saccadic eye movements (i.e. predicted MEG).

For this, we projected the classifier weights into source-space for both MEG data and predicted MEG data based on saccadic eye movements. We then averaged the weights across the significant cluster for MEG regularity decoding between 100 and 190 ms. The weights were normalised, meaning that while the absolute magnitudes of MEG and predicted MEG weights cannot be directly compared, the relative importance of their spatial patterns can still be meaningfully interpreted. This allows us to assess how similar brain regions contribute to the encoding of regularity across both general neural activity and oculomotor-related processes.

For MEG, the classifier weights indicated that informative activity primarily originated from the auditory cortices, showing a dominance in the right hemisphere (see Fig. 5C). In contrast, for predicted MEG, informative activity was mainly associated with parietal areas, also with a right-hemispheric dominance. The difference between MEG and predicted MEG reflects this shift, with MEG weights highlighting more informative activity in the right temporal regions, whereas predicted MEG emphasises the right parietal areas. Arguably more importantly for our proof-of-principle, the overlap results indicated substantial similarity in patterns between MEG and predicted MEG - particularly in midbrain, temporal, and parietal regions. This suggests that ocular action may play a role in shaping some of the responses to auditory events at these regions.

Finally, we assessed the extent to which eye features could be decoded from task-related neural data during the passive listening task, using whole-brain information. These predictions were generated by convolving task-related, source-projected brain data from both regularity conditions (ordered and random) with source-projected Ocular Response Functions (ORFs) originally derived from resting-state activity. The decoding accuracy was evaluated by comparing the actual eye feature's time series to the predictions generated from the neural data. To quantify performance, we calculated Pearson's correlation coefficients (*r*) for horizontal gaze, vertical gaze, and pupil dilation, and used Matthew's Correlation Coefficient (*MCC*) for blinks and saccades, following the same approach as in the resting-state analysis.

Overall, ocular behaviour was reliably decoded across all eye features and regularity conditions, even from task-related neural activity, except for vertical gaze in ICA-cleaned recordings, where decoding effects did not reach statistical significance (no-ICA, see Fig. 4a; ICA, see Fig. 4b). For summary statistics, please refer to the Supplementary Material (Supplementary Tables, Table 6-7).

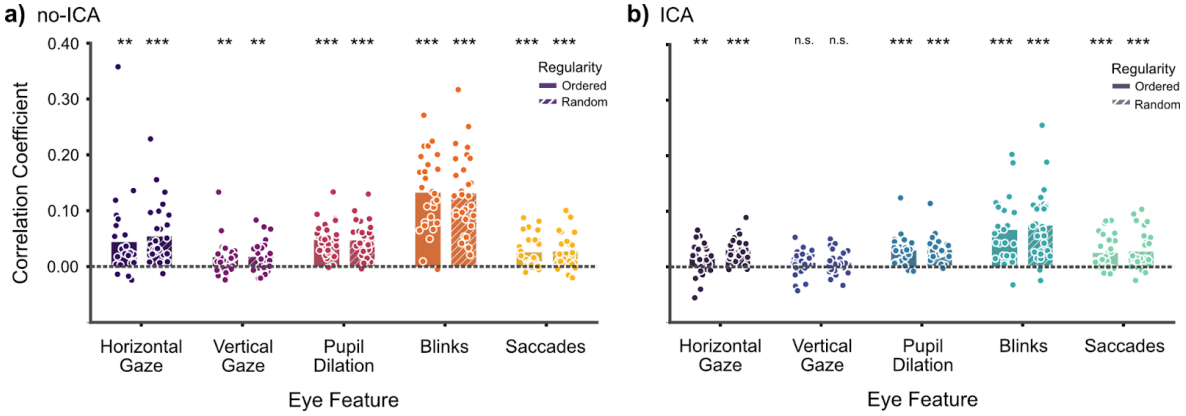

Fig. 6: *Ocular actions can be reliably decoded from task-related neural activity using source-projected ORFs*. We assessed the ability to decode eye features from task-related neural activity during the passive listening task by convolving source-projected brain data from both regularity conditions (ordered and random) with ORFs derived from resting-state activity. Eye features were reliably decoded across all features and conditions, except for vertical gaze in ICA-cleaned data, where decoding did not reach significance. a) No-ICA: Ordered: Horizontal Gaze (r = 0.04, p = 0.003), Vertical Gaze (r = 0.02, p = 0.007), Pupil Dilation (r = 0.05, p < 0.001), Blinks (MCC = 0.13, p < 0.001), Saccades (MCC = 0.03, p < 0.001). Random: Horizontal Gaze (r = 0.05, p < 0.001), Vertical Gaze (r = 0.02, p = 0.002), Pupil Dilation (r = 0.05, p < 0.001), Blinks (MCC = 0.13, p < 0.001), Saccades (MCC = 0.03, p < 0.001). b) ICA: Ordered: Horizontal Gaze (r = 0.01, p = 0.008), Vertical Gaze (r = 0.01, p = 0.072), Pupil Dilation (r = 0.03, p < 0.001), Blinks (MCC = 0.07, p < 0.001), Saccades (MCC = 0.02, p < 0.001). Random: Horizontal Gaze (r = 0.03, p < 0.001), Vertical Gaze (r = 0.01, p = 0.119), Pupil Dilation (r = 0.03, p < 0.001), Blinks (MCC = 0.07, p < 0.001), Saccades (MCC = 0.04, p < 0.001). Statistics were performed using one-sample Student's t-tests. 'n.s.': not significant; '*': p < 0.05; '**': p < 0.01; '***': p < 0.001. N = 28.

These results demonstrate that ORFs generalise effectively to task-related neural activity, enabling reliable decoding of ocular actions. This validation of the approach highlights the robustness of ORFs in capturing relevant oculomotor dynamics in neural signals across tasks and experimental settings. However, it should be noted that decoding vertical gaze from ICA-cleaned data did not reach statistical significance, arguably due to the reduced occurrence of vertical eye movements during resting-state, where participants were less likely to engage in such behaviours.

Discussion

The 'Ocular Response Function' provides a powerful tool for unravelling the complex role of oculomotor-related signals in human cognition and health. It characterises spatially and temporally precise transfer functions from ocular actions to neural activity and vice versa. We demonstrated that this approach reliably predicts brain activity from various eye features, and vice versa, while revealing insights into the spatial distribution of these effects across different brain regions and tasks as well as the idiosyncratic temporal patterns associated

with them. Furthermore, we demonstrated that this method can be used to gain deeper insights into cognitive processes, revealing the intricate interplay between oculomotor actions and neural activation patterns that might otherwise remain undetected.

Building on the functionality of temporal response functions (TRFs [36,38,39]), the ORF method establishes a continuous, time-resolved relationship between eye features and brain activity. By fitting these models to resting-state data, the approach enables precise mapping of the oculomotor-neural relationship across both spatial and temporal dimensions without the confounds of concurrent sensory events or task changes. Crucially, these time-resolved linear transfer functions enable the direct application of resting-state derived ORFs to other experimental tasks by convolving the ORFs with corresponding eye or brain recordings. This method marks a significant advance over previous approaches that aimed to deconvolve overlapping covariates (e.g. button presses, saccades) to neural or other physiological signals (e.g. pupil response) [40] by elucidating - rather than removing - the influence of these processes. It also extends work that linked subsets of eye features (i.e. pupil dilation) to neural dynamics during the resting-state [41] or aimed to decode gaze behaviour from various viewing conditions using deep neural networks [42]. By utilising an array of ocular actions and simple linear transformations, ORFs provide a more interpretable and efficient method to understand the links between neural processes and cognition.

ORFs offer great flexibility and can be tailored according to the level of specificity that is appropriate for different research questions and fields. For example, we projected ORFs into source space and applied PCA to extract the spatial and temporal components that account for the most variance within participants. This approach provided a comprehensive overview of how oculomotor activity in different brain areas relates to various eye features across multiple time scales. Conversely, in recording setups like EEG, where precise source localization is more challenging, analyses can still focus on electrodes of interest over broader topographic regions. Additionally, our open-source ORFs could be leveraged by research groups that lack the capability to collect both eye-tracking and brain recordings - determining likely eye patterns on the basis of the neural recordings only, or likely neural recordings solely on the basis of the ocular actions. This includes complex experiments or naturalistic settings where eye-tracking is challenging, and even recordings where participants' eyes are closed, such as during sleep. The ability to retrospectively assess the contribution of oculomotor processes to brain activity offers a major advantage, allowing for a deeper understanding of oculomotor contributions without the need for simultaneous eye-tracking data collection.

Classification of regularity conditions using both neural data and saccade-related neural activity during a passive listening task revealed that similar brain areas contribute to classification performance, with an overlap in weight patterns specifically over midbrain-temporal regions. This suggests that oculomotor processes may in principle contribute to the neural patterns seen during the task. The overlap highlights the potential of ORFs to isolate and examine the contribution of ocular actions to a range of neural responses, offering deeper insights into how brain activity related to experimental manipulations, or more complex, naturalistic environments, may be influenced by oculomotion. Furthermore, the successful application of ORFs to the passive listening task suggests that this method generalises beyond resting-state data, highlighting its flexibility for a wide range of experimental contexts. Generic ORFs, averaged across larger participant samples, could provide researchers with a powerful tool to estimate brain activity related to oculomotor or oculomuscular processes. This approach can reveal contrasts in brain regions like the visual or parietal cortex, or even hippocampal areas, offering insights into how different cognitive tasks, such as those involving working memory or attentional load, or even broader domain-general contributions to (action) perception [43], are influenced by oculomotion. Such insights could prompt the re-evaluation of previously reported neural effects that may have been partially driven by oculomotor activity.

We demonstrated that various features of ocular behaviour - namely horizontal and vertical gaze, pupil dilation, blinks, and saccades - are closely linked to brain areas including the frontal, visual, and parietal regions, as well as cerebellar, subcortical, and brainstem structures. These couplings largely persisted even after removing scalp signal variance related to ocular muscle activity using ICA. Notably, the first principal components of the ORFs for no-ICA vs ICA encoding showed a topographic shift from frontal regions to more occipital, cerebellar, and subcortical areas, along with a delayed neural response. Only for saccadic eye movements, ICA correction did not seem to clearly change the spatial or temporal pattern of the first component. Possibly, the variance representing the relationship between neural activity and saccadic movements was already accounted for by other covariates in the model, such as gaze and blinks. However, these findings are consistent with recent evidence suggesting that viewing behaviour plays a significant role in various cognitive effects [2–14] and may even influence cerebellar activity, particularly in complex task designs [44]. Additionally, other studies have demonstrated close links between eye movements and peripheral auditory processing through a midbrain-level hub [45–48], which may also be partly captured by components loading on these regions. A region-of-interest-based approach using ORFs could further provide valuable insights into subcortical or brainstem

mappings between oculomotion and neural activity, areas that are especially challenging to investigate in non-invasive studies.

Components also exhibited individual variability, which could provide valuable insights into interindividual differences in brain function, particularly in how neural representations or activations are translated into oculomotor actions. This could complement and extend recent work demonstrating that individual variability in neurophysiological activity can provide meaningful insights into brain function and personalised neural signatures [49,50]. Additionally, this variability may contribute to behavioural differences not only in healthy individuals but also in those with psychopathology or neurological disorders. Importantly, the ORF provides a quantitative metric of neuronal system integrity that can be directly assessed in patient populations. In contrast to pure resting state data these additional deterministic metrics (based on physical movement and the neuronal activity that underlies it) may give a much clearer differentiation between cohorts. For example, differences in pupil dilation ORFs between patients with dementia or Parkinson's disease and healthy controls, either through a PCA-based approach or by targeting specific brain regions such as the locus coeruleus, could offer fundamental insights into aberrant neural functioning and associated behavioural outcomes. A brief resting-state measurement followed by ORF estimation could significantly enhance our understanding, early detection, and diagnosis of these disorders.

In summary, the Ocular Response Function (ORF) provides a powerful and flexible tool for investigating the intricate relationship between oculomotor behaviour and neural activity. By enabling the prediction of brain activity from eye movements (and vice versa), ORFs offer novel insights into how different brain regions contribute to cognitive processes across diverse tasks. They reveal spatial and temporal patterns that might otherwise remain undetected, demonstrating the potential to advance research in both typical cognition and in clinical contexts, where ORFs could shed light on individual variability and pathological conditions.

Methods

This manuscript used data acquired by Schubert et al. [34]. In the following, we provide a detailed description of materials and methods that are required for the understanding of the current work.

Participants

We used data from 29 participants (12 female, 17 male; mean age = 25.70, range = 19 - 43). For the passive listening task, the eye tracker failed to detect the pupil and corneal reflection for one participant, leading to a flat signal for the majority of one block. As a result, no valid data were recorded for that block and the participant was excluded from the analysis, leaving a total of 28 participants for the passive listening task. All participants reported normal hearing and had normal, or corrected to normal, vision. They gave written, informed consent and reported that they had no previous neurological or psychiatric disorders. The experimental procedure was approved by the ethics committee of the University of Salzburg and was carried out in accordance with the declaration of Helsinki. All participants received either a reimbursement of 10 € per hour or course credits.

Stimuli and Experimental Design

We assessed participants' head shapes before the start of the experiment using cardinal head points (nasion and pre-auricular points), digitised with a Polhemus Fastrak Digitiser (Polhemus), and around 300 points on the scalp. For all parts of the experiment, for both the resting-state period and the passive tone listening task, participants were instructed to direct their gaze toward a black cross at the centre of a screen. Each MEG session then started with a 5-minute resting-state recording. Afterwards, the individual hearing threshold was determined using a pure tone of 1043 Hz. This was followed by 2 blocks of passive listening to tone sequences of varying entropy levels. Sequences consisted of four different pure tones (f1: 440 Hz, f2: 587 Hz, f3: 782 Hz, f4: 1043 Hz, each lasting 100 ms), each block consisted of 1500 tones presented with a temporally predictable rate of 3 Hz. Entropy levels (ordered / random) changed pseudorandomly every 500 trials within each block, thus resulting in a total of 1500 trials per entropy condition. While in an “ordered” context forward transitions (i.e. f1→f2, f2→f3, f3→f4, f4→f1) had a high probability of 75%, repetitions (e.g., f1→f1, f2→f2,...) were rather unlikely with a probability of 25%. However, in a “random” context all possible transitions (including forward transitions and repetitions) were equally likely with a probability of 25%.

Data Acquisition and Preprocessing

MEG. We collected MEG data using a whole head system (Elekta Neuromag Triux, Elekta Oy, Finland), placed within a standard passive magnetically shielded room (AK3b, Vacuumschmelze, Germany). The signal was recorded with 102 magnetometers and 204 orthogonally placed planar gradiometers at 102 different positions at a sampling frequency of

1 kHz (hardware filters: 0.1 - 330 Hz). In a first step, a signal space separation algorithm, implemented in the Maxfilter program (version 2.2.15) provided by the MEG manufacturer, was used to clean the data from external noise and realign data from different blocks to a common standard head position. Data preprocessing was performed using Matlab R2020b (The MathWorks, Natick, Massachusetts, USA) and the FieldTrip Toolbox (Oostenveld et al., 2011). All data were band-pass filtered between 0.5 Hz and 30 Hz (onepass-zerophase finite impulse response (FIR) filter, order 3330, hamming-windowed) and downsampled to 100 Hz. We further used two versions of preprocessed data that either used independent component analysis to reject eye movement (and heart-rate) related artefacts or not. We further refer to these data as either ICA or no-ICA respectively. For ICA, to identify eye movement and heart rate artefacts, 65 independent components were identified from filtered (onepass-zerophase lowpass FIR filter, order 132, hamming-windowed; onepass-zerophase highpass FIR filter, order 1650, hamming-windowed) continuous data of the resting-state recordings using runica-ICA. Components originating from eye movements and heartbeat were then identified by visual inspection of component topographies and time-courses and removed (median = 3 components, min = 2, max = 4).

Eye Tracking. We used a Trackpixx3 binocular tracking system (Vpixx Technologies, Canada) with a 50 mm lens. We synchronised MEG and eye-tracking data feeding the Trackpixx's output data as three additional channels into the MEG system, representative of horizontal gaze, vertical gaze, and pupil dilation of participants' right eye. Recordings started after a 13-point calibration and validation procedure. Throughout the experiment participants were seated in the MEG at a distance of 82 cm from the screen, with their chin resting on a chinrest to reduce head movements. We used an algorithm based on pupillometry noise to detect blinks [51]. To account for potential residual blink artefacts, we removed an additional 30 ms around blink edges for gaze and 100 ms for pupil dilation data. Blinks were then removed from gaze and pupil dilation data and linearly interpolated. For saccade detection, we used a velocity-based detection approach [2–4] using the Euclidean distance between successive gaze points in the horizontal and vertical planes as in [5] with a 7 ms smoothing window on the resulting velocity vector (using the built "smoothdata" function in Matlab), thus considering two-dimensional velocity profiles. Saccade on-/offsets (i.e. durations) were then identified where velocity exceeded and subsequently fell below the threshold of five times the median velocity. A minimum delay of 100 ms was used between saccade onsets to prevent multiple detections of the same saccade. We additionally excluded saccades from pupil dilation data and linearly interpolated the gaps. For further analysis, blinks and saccades were transformed into binary vectors of zeros (no blink/saccade) and ones (blink/saccade) retaining event durations. Afterwards, horizontal and vertical gaze data were bandpass

filtered between 0.1 - 10 Hz (onepass-zerophase finite impulse response (FIR) filter, order 16500, hamming-windowed), pupil dilation data were bandpass filtered between 0.01 - 4 Hz (onepass-zerophase finite impulse response (FIR) filter, order 165000, hamming-windowed), then both gaze and pupil dilation were median centred on the screen centre. Finally, eye tracking data were appended as five individual channels to the MEG data and therefore downsampled to 100 Hz alongside the MEG data. Note that binary blink and saccade vectors were then restored by adding "1 s" at the nearest time points of the original sampling rate to avoid potential data loss of short activation patterns (i.e. onsets).

MEG and Eye Tracking. Resting-state data were cut from 10 s to 290 s after recording onset. Data of the entropy modulation paradigm were cut from -1 s of the first tone to +1 s of the last tone of every 500 tone segment and corrected for a 16 ms delay between trigger and stimulus onset generated by sound travelling through the pneumatic headphones into the shielded MEG room.

The Ocular Response Function

Encoding Models. To establish transfer functions from oculomotor action to neural representations, we estimated a multivariate temporal response function (mTRF) using the Eelbrain toolkit [36]. A deconvolution algorithm [35] (boosting) was applied to the resting state data to estimate the optimal TRFs that predict the brain activity of 306 MEG sensors (dependent variable) from eye features (predictors), i.e. horizontal gaze, vertical gaze, pupil dilation, blinks, and saccades. Please note that we deliberately chose boosting over ridge regression [38,39] to estimate TRFs as it imposes a sparse prior, hence encouraging TRFs with fewer non-zero elements. This sparsity helps focus on the core components of the signal, minimising irrelevant fluctuations which becomes especially relevant considering effective 'ocular response function' filters. For model fitting, all sensors of the dependent variable as well as the predictors were separately centred around zero and standardised against the standard deviation. The defined time-lags to train the model were from -1 s to 1 s. We further used a 100 ms wide Hamming window basis function (please refer to [36] for further details on the boosting algorithm and parameters). To evaluate the model, the data was split into 4 folds, and a cross-validation approach was used to avoid overfitting [52]. All predictors were included into the same encoding model. Therefore, to avoid stopping the entire model training when a single predictor starts overfitting, we used selective stopping ("selective_stopping = True" in eelbrain's boosting function) which "allows freezing only the predictor which caused the overfitting, while training of the TRF components corresponding to the remaining predictors continues, until all predictors are frozen" [36].

This results in different response functions (depending on the amount of different input features) that best describe how each eye feature is translated into a neural activation pattern at each individual MEG sensor. Crucially, each filter can then simply be reversed in time and used to result in a backward decoding model, i.e. predicting eye features from brain activity:

Decoding Models. We then iterated over each eye feature's response function for each of the 306 MEG sensors and simply flipped their direction along the time axis. This effectively generates response functions to predict oculomotor activity from brain data, similar to a backward decoding approach.

When applicable, we can then gain insights into the spatial components that drive this relationship and project the ORFs into source space (see Source Projection). Please note that for further model evaluation it is necessary to also project the response variable, i.e. brain activity, into source space.

Since eye blinks and saccades were originally represented as binary predictors, we converted the predicted continuous blink and saccade data into binary variables. Following an approach similar to neural spike analyses, we applied a sigmoid function to the continuous predictions, converting them into probabilities. These probabilities were thresholded, with values greater than 0.5 classified as '1' and others as '0'. We then used the Matthews correlation coefficient (MCC) to compare the predicted binary labels to the ground truth binary labels and assess model performance [53,54]. For decoding model evaluation, Pearson correlation was used for continuous variables (horizontal gaze, vertical gaze, pupil dilation), and MCC was used for binary variables (blinks, saccades).

Source projection

ORFs of all 306 MEG sensors were therefore further projected into source-space using LCMV spatial filters [55]. LCVM filters were computed by warping anatomical template images to the individual head shape and further brought into a common space by co-registering them based on the 3 anatomical landmarks (nasion, left, and right preauricular points) with a standard brain from the Montreal Neurological Institute (MNI, Montreal, Canada; [56]). Then, we computed a single-shell head model [57] for each participant. As a source model, a grid with 1 cm resolution and 2982 voxels based on an MNI template brain was morphed into the brain volume of each participant. This allowed group-level averaging and statistical analysis

as all the grid points in the warped grid belong to the same brain region across subjects. Spatial filters were estimated by following a publicly available tutorial that was made available by FieldTrip and can be found on their homepage (https://www.fieldtriptoolbox.org/workshop/paris2019/handson_sourceanalysis/). In short, the 306 MEG sensor data were prewhitened to account for rank deficiency of the data caused by independent component analysis (ICA) and / or signal space projections (SSPs) [58]. For prewhitening, we used the implemented “ft_denoise_prewhiten” function with a kappa value that was based on the first large 'cliff' in the singular value spectrum of the covariance matrix of the gradiometers and magnetometers respectively. (Please note that kappa is the number at which the singular value spectrum of the covariance matrix will be truncated). The forward model, i.e. leadfield (normalised), was then computed based on the updated gradiometer structure of the prewhitened data. Then, spatial filters were computed using a kappa value based on the first large 'cliff' in the singular value spectrum of the covariance matrix of prewhitened data. In order to create spatial filters, this step was repeated with resting-state data sets where ICA component rejection has or has not been applied, resulting in two different spatial filter matrices. Respective filter matrices were then used to project ORFs, resting state brain activity, and entropy modulation paradigm brain activity into source space (using the ICA & no-ICA resting state filter matrices). Anatomical labels were obtained using the automated anatomical labelling atlas 3 (AAL3; [59]). Wherever the coordinates of an effect in mni-space did not correspond to any labelled region, nearest neighbour interpolation was applied. This approach allowed for the assignment of unlabeled coordinates by identifying the closest labelled region.

Principal component analysis

To reduce the number of statistical comparisons and identify the most relevant components of the neural response across source space and time, we applied principal component analysis (PCA) to transform the 2982-voxel space into an orthogonal component space based on individual source-projected ORFs. This process condensed the high-dimensional data into key components that capture the most variance in the brain's response to eye movements, thereby focusing the analysis on the critical aspects of the ocular-brain relationship. To mitigate potential regression artefacts, we cropped ORF edges to time lags between -0.9 and 0.9 seconds. As there was no particular interest in dipole orientation in the current case, we disregarded sensor polarity and calculated the absolute value of the cropped ORFs. We extracted the weight matrices for the first three components and multiplied them by individual ORFs (for each eye feature, for both no-ICA and ICA) to derive the source locations and temporal profiles of the ORF components. The projected data for

each subject was subsequently used for the decoding analysis. For consistency, we selected the first three principal components based on the maximum explained variance within each eye feature for each preprocessing condition (no-ICA vs. ICA) for each participant, avoiding methods like visual inspection of the “elbow” in the ranked cumulative explained variance plot to determine the optimal number of components.

Multivariate Pattern Analysis (MVPA)

To gain deeper insights into how oculomotor activity may influence neural activation patterns during experimental tasks, we applied the resting-state derived ORFs to data from a passive listening paradigm (see Fig. 5A). This analysis used ICA-cleaned data across all participants. Given recent findings linking neural excitability in the auditory cortex with saccades [37], we focused on potential overlaps with saccade-related neural activity. We convolved each participant's saccadic eye movement data from the task with sensor-based saccade ORFs, generating predicted MEG (Saccades) data for 306 sensors.

Both the ICA-cleaned MEG and predicted MEG data were epoched around tone onsets (-0.1 to 0.4 seconds), resulting in 3000 epochs (1500 for the ordered regularity condition and 1500 for the random condition). The data were subjected to time-resolved classification using the MVPA-Light package [60]. We employed the default 5-fold cross-validation, z-scoring as a preprocessing step, and linear discriminant analysis (LDA) to decode regularity conditions (i.e. ordered vs. random) from both MEG and predicted MEG data, as well as a shuffled version of those labels as a control. This process yielded one accuracy value per time point and one classifier weight per time point per sensor for each participant.

Classifier weights were corrected by their covariance structure [61], projected into source space by multiplying them with the resting-state spatial filters, and baseline-corrected (relative change) from -0.05 - 0 s [62] relative to tone onset. We then averaged these weights from 0.10 - 0.19 s (sig. Cluster of the MEG decoding, see Fig. 5B). To ensure comparability between true and predicted MEG results, whilst maintaining the relative importance of brain areas in sensitivity to changes in stimulus regularity, weights from both datasets were z-scored (i.e., standardised to a mean of 0 and standard deviation of 1). After this transformation, the negative of the minimum value across both datasets (i.e. global minimum) was added to retain zero values ($z' = z + (\min(z) * -1)$).

To explore the shared contributions of neural and oculomotor processes to regularity processing, we calculated both the difference and overlap of the averaged, normalised

classifier weights. The difference was computed by subtracting the predicted MEG weights ($Weights_{PredictedMEG}$) from the MEG weights ($Weights_{MEG}$). The overlap was computed according to the following formula:

$$((Weights_{MEG} + Weights_{PredictedMEG}) - abs(Weights_{MEG} - Weights_{PredictedMEG})) / 2$$

Statistical Analysis

For the statistical analysis of resting-state data, we employed one-sample Student's t-tests to evaluate the significance of the encoding and decoding correlation coefficients (see evaluation metrics). To obtain one encoding correlation coefficient for each participant, we first averaged the PCA weight matrices across participants and identified the voxel with the maximum component weight for each of the first three components. We then extracted the correlation coefficient from these peak locations for each participant. Subsequently, we report the r-values, t-values, p-values, and Cohen's d effect sizes for each one-sample Student's t-test. We intentionally chose to use one-sample t-tests over alternatives such as ANOVA or mixed-effects models, as we did not aim to assess whether one type of eye movement was more strongly represented in neural activity than another. Our primary interest was to demonstrate that ocular behaviour is consistently represented across various brain regions, allowing for reliable encoding and decoding effects, rather than exploring the extent of differences between them.

To statistically evaluate the MVPA analysis of the passive listening data, we used a cluster-based randomization approach. This analysis was conducted across all time points within the classifier time window (-0.1 to 0.4 seconds). Specifically, we tested two one-sided contrasts (see Fig. 5B), comparing classifier accuracy for true versus shuffled regularity condition labels (ordered vs. random). We computed the randomization distribution of t-values across 10,000 permutations, using a cluster-forming alpha threshold of 0.05. The resulting clusters were compared against the original contrast at an alpha level of 0.05, Bonferroni corrected. For each significant cluster, we report the average t-values, p-values, and Cohen's d (effect size) across the time points within the cluster. Decoded eye movements and the corresponding correlation coefficients were evaluated in the same manner as for the resting-state data.

Data availability

Preprocessed Data required to reproduce the analyses supporting this work will be publicly available upon publication. Raw data (> 250 GB) will be shared upon request.

Code availability

Code to analyse preprocessed data and further reproduce results and figures from this manuscript will be available upon publication.

Acknowledgements

Thanks to the whole research team. Special thanks to Manfred Seifter for his support in conducting the measurements, to Gareth Barnes for comments on the manuscript, and to the MEG group at the Functional Imaging Lab, UCL, for input on the idea. This work was supported by a Leverhulme Project Grant (RPG-2022-358) and European Research Council (ERC) consolidator grant (101001592) under the European Union's Horizon 2020 research and innovation programme, both awarded to C.P.

Author contributions

Q.G. designed the experiment, collected and analysed the data, generated the figures, and wrote the manuscript. J.S. designed the experiment, collected and analysed the data, and edited the manuscript. A.K. contributed to data analyses and edited the manuscript. N.W. collected the data, contributed to data analyses and edited the manuscript. C.P. acquired the funding, supervised the project, and edited the manuscript.

References

1. Shaikh, A. G. & Zee, D. S. Eye Movement Research in the Twenty-First Century—a Window to the Brain, Mind, and More. *The Cerebellum* **17**, 252–258 (2018).
2. Liu, B., Nobre, A. C. & van Ede, F. Functional but not obligatory link between microsaccades and neural modulation by covert spatial attention. *Nat. Commun.* **13**, 3503 (2022).
3. Liu, B., Nobre, A. C. & van Ede, F. Microsaccades transiently lateralise EEG alpha activity. *Prog. Neurobiol.* **224**, 102433 (2023).
4. de Vries, E., Fejer, G. & van Ede, F. No obligatory trade-off between the use of space and time for working memory. *Commun. Psychol.* **1**, 1–10 (2023).
5. De Vries, E. & Van Ede, F. Microsaccades Track Location-Based Object Rehearsal in

Visual Working Memory. *eneuro* **11**, ENEURO.0276-23.2023 (2024).

6. Gehmacher, Q. *et al.* Eye movements track prioritized auditory features in selective attention to natural speech. *Nat. Commun.* **15**, 3692 (2024).
7. Schubert, J., Gehmacher, Q., Schmidt, F., Hartmann, T. & Weisz, N. Prediction tendency, eye movements, and attention in a unified framework of neural speech tracking. *eLife* **13**, (2024).
8. Popov, T., Gips, B., Weisz, N. & Jensen, O. Brain areas associated with visual spatial attention display topographic organization during auditory spatial attention. *Cereb. Cortex* bhac285 (2022) doi:10.1093/cercor/bhac285.
9. Corbetta, M. & Shulman, G. L. Control of goal-directed and stimulus-driven attention in the brain. *Nat. Rev. Neurosci.* **3**, 201–215 (2002).
10. Corbetta, M. *et al.* A Common Network of Functional Areas for Attention and Eye Movements. *Neuron* **21**, 761–773 (1998).
11. Astafiev, S. V. *et al.* Functional Organization of Human Intraparietal and Frontal Cortex for Attending, Looking, and Pointing. *J. Neurosci.* **23**, 4689–4699 (2003).
12. Engbert, R. & Kliegl, R. Microsaccades uncover the orientation of covert attention. *Vision Res.* **43**, 1035–1045 (2003).
13. Hafed, Z. M. & Clark, J. J. Microsaccades as an overt measure of covert attention shifts. *Vision Res.* **42**, 2533–2545 (2002).
14. Madsen, J. & Parra, L. C. Bidirectional brain-body interactions during natural story listening. *Cell Rep.* **43**, 114081 (2024).
15. Rawal, A. & Rademaker, R. L. Visual exploration goes down with higher working memory load, while more saccades negatively impact recall. *J. Vis.* **24**, 383 (2024).
16. Lyu, H. *et al.* Eye Movement Abnormalities Can Distinguish First-Episode Schizophrenia, Chronic Schizophrenia, and Prodromal Patients From Healthy Controls. *Schizophr. Bull. Open* **4**, sgac076 (2023).
17. Morita, K., Miura, K., Kasai, K. & Hashimoto, R. Eye movement characteristics in schizophrenia: A recent update with clinical implications. *Neuropsychopharmacol. Rep.*

40, 2–9 (2020).

18. Broerse, A., Crawford, T. J. & den Boer, J. A. Parsing cognition in schizophrenia using saccadic eye movements: a selective overview. *Neuropsychologia* **39**, 742–756 (2001).
19. Wolf, A., Ueda, K. & Hirano, Y. Recent updates of eye movement abnormalities in patients with schizophrenia: A scoping review. *Psychiatry Clin. Neurosci.* **75**, 82–100 (2021).
20. Obyedkov, I. *et al.* Saccadic eye movements in different dimensions of schizophrenia and in clinical high-risk state for psychosis. *BMC Psychiatry* **19**, 110 (2019).
21. Caldani, S. *et al.* Saccadic eye movements as markers of schizophrenia spectrum: Exploration in at-risk mental states. *Schizophr. Res.* **181**, 30–37 (2017).
22. D'Antonio, F. *et al.* Blink Rate Study in Patients with Alzheimer's Disease, Mild Cognitive Impairment and Subjective Cognitive Decline. *Curr. Alzheimer Res.* **18**, 1104–1110 (2021).
23. Ladas, A., Frantzidis, C., Bamidis, P. & Vivas, A. B. Eye Blink Rate as a biological marker of Mild Cognitive Impairment. *Int. J. Psychophysiol.* **93**, 12–16 (2014).
24. Molitor, R. J., Ko, P. C. & Ally, B. A. Eye Movements in Alzheimer's Disease. *J. Alzheimers Dis. JAD* **44**, 1–12 (2015).
25. Granholm, E. L. *et al.* Pupillary Responses as a Biomarker of Early Risk for Alzheimer's Disease. *J. Alzheimers Dis. JAD* **56**, 1419–1428 (2017).
26. Zeeman, M. *et al.* Task-Evoked Pupillary Response as a Potential Biomarker of Dementia and Mild Cognitive Impairment: A Scoping Review. *Am. J. Alzheimers Dis. Dementias®* **38**, 15333175231160010 (2023).
27. Brendler, A. *et al.* Assessing hypo-arousal during reward anticipation with pupillometry in patients with major depressive disorder: replication and correlations with anhedonia. *Sci. Rep.* **14**, 344 (2024).
28. Wen, M. *et al.* Depression and Cognitive Impairment: Current Understanding of Its Neurobiology and Diagnosis. *Neuropsychiatr. Dis. Treat.* **18**, 2783–2794 (2022).
29. Schneider, M. *et al.* Pupil Dilation during Reward Anticipation Is Correlated to

Depressive Symptom Load in Patients with Major Depressive Disorder. *Brain Sci.* **10**, 906 (2020).

30. Carvalho, N. *et al.* Saccadic Eye Movements in Depressed Elderly Patients. *PLoS ONE* **9**, e105355 (2014).
31. Whittaker, C. K. Tinnitus and eye movement. *Am. J. Otol.* **4**, 188 (1982).
32. Lockwood, A. H. *et al.* The functional anatomy of gaze-evoked tinnitus and sustained lateral gaze. *Neurology* **56**, 472–480 (2001).
33. Simmons, R., Dambra, C., Lobarinas, E., Stocking, C. & Salvi, R. Head, Neck, and Eye Movements That Modulate Tinnitus. *Semin. Hear.* **29**, 361–370 (2008).
34. Schubert, J., Gehmacher, Q., Schmidt, F., Hartmann, T. & Weisz, N. Prediction tendency, eye movements, and attention in a unified framework of neural speech tracking. 2023.06.27.546746 Preprint at https://doi.org/10.1101/2023.06.27.546746 (2024).
35. David, S. V., Mesgarani, N. & Shamma, S. A. Estimating sparse spectro-temporal receptive fields with natural stimuli. *Netw. Bristol Engl.* **18**, 191–212 (2007).
36. Brodbeck, C. *et al.* Eelbrain, a Python toolkit for time-continuous analysis with temporal response functions. *eLife* **12**, e85012 (2023).
37. Leszczynski, M. *et al.* Saccadic modulation of neural excitability in auditory areas of the neocortex. *Curr. Biol.* **33**, 1185-1195.e6 (2023).
38. Crosse, M. J., Di Liberto, G. M., Bednar, A. & Lalor, E. C. The multivariate temporal response function (mTRF) toolbox: a MATLAB toolbox for relating neural signals to continuous stimuli. *Front. Hum. Neurosci.* **10**, 604 (2016).
39. Crosse, M. J. *et al.* Linear modeling of neurophysiological responses to speech and other continuous stimuli: methodological considerations for applied research. *Front. Neurosci.* **15**, (2021).
40. Ehinger, B. V. & Dimigen, O. Unfold: an integrated toolbox for overlap correction, non-linear modeling, and regression-based EEG analysis. *PeerJ* **7**, e7838 (2019).
41. Pfeffer, T. *et al.* Coupling of pupil- and neuronal population dynamics reveals diverse influences of arousal on cortical processing. *eLife* **11**, e71890 (2022).

42. Frey, M., Nau, M. & Doeller, C. F. Magnetic resonance-based eye tracking using deep neural networks. *Nat. Neurosci.* **24**, 1772–1779 (2021).
43. Press, C. & Cook, R. Beyond action-specific simulation: domain-general motor contributions to perception. *Trends Cogn. Sci.* **19**, 176–178 (2015).
44. Zoefel, B., Abbasi, O., Gross, J. & Kotz, S. A. Entrainment echoes in the cerebellum. *Proc. Natl. Acad. Sci.* **121**, e2411167121 (2024).
45. Bulkin, D. A. & Groh, J. M. Distribution of eye position information in the monkey inferior colliculus. *J. Neurophysiol.* **107**, 785–795 (2012).
46. King, C. D. *et al.* Individual similarities and differences in eye-movement-related eardrum oscillations (EMREOs). *Hear. Res.* **440**, 108899 (2023).
47. Lovich, S. N. *et al.* Parametric information about eye movements is sent to the ears. *Proc. Natl. Acad. Sci.* **120**, e2303562120 (2023).
48. Porter, K. K., Metzger, R. R. & Groh, J. M. Visual- and saccade-related signals in the primate inferior colliculus. *Proc. Natl. Acad. Sci.* **104**, 17855–17860 (2007).
49. da Silva Castanheira, J., Orozco Perez, H. D., Misic, B. & Baillet, S. Brief segments of neurophysiological activity enable individual differentiation. *Nat. Commun.* **12**, 5713 (2021).
50. Dubois, J. & Adolphs, R. Building a Science of Individual Differences from fMRI. *Trends Cogn. Sci.* **20**, 425–443 (2016).
51. Hershman, R., Henik, A. & Cohen, N. A novel blink detection method based on pupillometry noise. *Behav. Res. Methods* **50**, 107–114 (2018).
52. Ying, X. An Overview of Overfitting and its Solutions. *J. Phys. Conf. Ser.* **1168**, 022022 (2019).
53. Chicco, D. & Jurman, G. The Matthews correlation coefficient (MCC) should replace the ROC AUC as the standard metric for assessing binary classification. *BioData Min.* **16**, 4 (2023).
54. Chicco, D. & Jurman, G. The advantages of the Matthews correlation coefficient (MCC) over F1 score and accuracy in binary classification evaluation. *BMC Genomics* **21**, 6

(2020).

55. Van Veen, B. D., Van Drongelen, W., Yuchtman, M. & Suzuki, A. Localization of brain electrical activity via linearly constrained minimum variance spatial filtering. *IEEE Trans. Biomed. Eng.* **44**, 867–880 (1997).
56. Mattout, J., Henson, R. N. & Friston, K. J. Canonical Source Reconstruction for MEG. *Comput. Intell. Neurosci.* **2007**, e67613 (2007).
57. Nolte, G. The magnetic lead field theorem in the quasi-static approximation and its use for magnetoencephalography forward calculation in realistic volume conductors. *Phys. Med. Biol.* **48**, 3637 (2003).
58. Westner, B. U. *et al.* A unified view on beamformers for M/EEG source reconstruction. *NeuroImage* **246**, 118789 (2022).
59. Rolls, E. T., Huang, C.-C., Lin, C.-P., Feng, J. & Joliot, M. Automated anatomical labelling atlas 3. *NeuroImage* **206**, 116189 (2020).
60. Treder, M. S. MVPA-Light: A Classification and Regression Toolbox for Multi-Dimensional Data. *Front. Neurosci.* **14**, (2020).
61. Haufe, S. *et al.* On the interpretation of weight vectors of linear models in multivariate neuroimaging. *NeuroImage* **87**, 96–110 (2014).
62. Demarchi, G., Sanchez, G. & Weisz, N. Automatic and feature-specific prediction-related neural activity in the human auditory system. *Nat. Commun.* **10**, 3440 (2019).